ORIGINAL RESEARCH **Open access**

Receding Horizon Distributed Motion Planning for Quadrotors under Wind Disturbances

Sven Larsson[1*], Erik Johansson[2], Anna Nilsson[3], Lars Andersson[4]

Abstract

This study shows distributed motion planning for multi-rotor unmanned aerial vehicles operating in windy outdoor settings. The motion planning task is formulated as a receding-horizon mixed-integer nonlinear programming (RH-MINLP) problem. Every quadrotor independently solves an RH-MINLP to create its time-optimal speed profile along a minimum snap spline trajectory, while meeting all constraints involving kinematics, dynamics, communication connectivity, and collision avoidance. Due to wind disturbances, the motion planner must frequently produce updated plans, which greatly raises computational load and can risk safety breaches. Control Barrier Functions (CBFs) are introduced to aid collision avoidance despite wind effects and to lessen the need for ongoing recalculation of motion plans. The RH-MINLPs are solved using an innovative blend of heuristic and optimal solvers—Simulated Annealing and interior-point methods—to efficiently handle discrete variables and nonlinear constraints in real time. The overall framework is validated through simulations with up to 50 quadrotors, Hardware-in-the-Loop (HWIL) tests, and real outdoor trials involving up to 6 DJI M100 quadrotors. Findings confirm (1) rapid online motion planning for outdoor communication-centric multi-quadrotor missions and (2) the value of CBFs for generating robust motion plans.

Keywords Quadrotor motion planning, Multi-UAV systems, Mathematical optimization, Control barrier functions, Dryden wind model

*Correspondence:
Sven Larsson
sven.larsson@slu.se
[1] Department of AI for Precision Forage and Silage Quality, Faculty of Agriculture, Swedish University of Agricultural Sciences, Uppsala, Sweden
[2] Department of Machine Learning for Crop Rotation Planning, Faculty of Agriculture, KTH Royal Institute of Technology, Stockholm, Sweden
[3] Department of Smart Tractor Autonomy, Faculty of Agriculture, Lund University, Lund, Sweden
[4] Department of Precision Soil pH Mapping, Faculty of Agriculture, University of Gothenburg, Gothenburg, Sweden

Introduction

Safe and dependable motion and formation coordination of networked multi-rotor unmanned aerial vehicles (UAVs) for applications such as surveillance and cargo transport faces limitations from UAV kinematics and dynamics, external factors such as wind gusts and shear, and the need to prevent collisions [1].

Following the early contributions of Schouwenaars *et al.* [2] and Richards and How [3], the literature on centralized and decentralized Mathematical Programming (MP) or Mathematical Optimization techniques for multi-vehicle motion planning problems (MVMPs) has continued to expand across ground [4, 5], underwater [6, 7], and aerial robotic platforms [8, 9]. Mixed-integer nonlinear programs (MINLPs) prove capable of encompassing all MVMP constraints. However, solving these MINLPs for MVMP scenarios remains highly demanding computationally (NP-hard), making real-time execution and large-scale use difficult [10]. A practical solution to this issue involves receding horizon (RH) or model

This is an open access article distributed under the terms of the Creative Commons Attribution-NonCommercial-ShareAlike 4.0 International License (CC BY-NC-SA 4.0), which permits non-commercial use, distribution, reproduction, and adaptation in any medium or format, provided that appropriate credit is given to the original author(s) and source, a link to the license is provided, and any changes made are indicated. Adapted material must be distributed under the same license.

© 2025 The Author(s). | Published by Agro Intelligence Research Press

predictive control (MPC) strategies. Such techniques have demonstrated strong performance for online and real-time motion planning in multi-robot teams operating in dynamic, partially known environments [11, 12]. One significant strength of MP-based strategies lies in their capacity to analyze the balance among mobility (speed, acceleration, waypoints), wireless communications (bandwidth, buffer size, path loss, delay), and energy requirements [8, 13]. This research evaluates a distributed MINLP-based motion planner for multiple quadrotors, in which each vehicle calculates its future path locally and exchanges it with the others. **Figure 1** illustrates snapshots of multiple quadrotors taken during outdoor flight tests.



Figure 1. Snapshots of quadrotors flying in different flight formations, namely straight line (2 quadrotors—top left), rectangle (6 quadrotors—top right), and triangle (3 quadrotors—bottom left). The bottom-right image shows an FT-205 wind sensor mounted on the DJI Matrice 100 quadrotor to collect real-time wind data during a flight test.

For quadrotors working in outdoor conditions, solving MVMPs grows considerably harder when wind disturbances are present. While much research addresses multi-quadrotor motion planning, only recent publications have explored simulation or experimental techniques specifically designed to address wind-gust countermeasures [14-17]. Simulation-based studies apply wind models, such as the Dryden and Von Kármán models, to incorporate realistic gusts into the planning process [18, 19]. Experimental efforts estimate wind speed and direction using devices such as ultrasonic anemometers, pitot tubes, accelerometers, gyroscopes, and barometers [20]. This work applies the Dryden model to generate realistic wind gusts within both simulations and Hardware-in-the-Loop (HWIL) experiments.

Wind gusts repeatedly displace quadrotors from their planned locations, creating the demand for quick recalculation of MP solutions to avoid greater collision hazards [21]. Frequent recomputations hinder the practical value of MP-based systems in windy environments. Therefore, an innovative method is necessary to reduce the need for repeated MP solving without sacrificing mission safety. This study proposes a new MINLP solving technique that integrates heuristic and optimal approaches—specifically, simulated annealing and interior-point methods—to address discrete variables and nonlinearities in a manner suitable for real-time applications.

© 2025 The Author(s). | Published by Agro Intelligence Research Press

Control Barrier Functions (CBFs) continue to see growing use for achieving reliable collision avoidance across multi-vehicle platforms [22]. These functions have been successfully deployed in individual UAV tasks to maintain safe separation during cave exploration missions, seamlessly integrating with established motion control systems [23]. In addition, CBFs have enabled safe, collision-free coordination for groups of quadrotors in both indoor and outdoor conditions, supporting formation maintenance and protected human-in-the-loop teleoperation [24-26]. Although promising, the actual robustness of CBFs fluctuates notably with the level of intrusiveness introduced by the barrier constraint [27]. The present work builds on prior efforts by incorporating CBFs to handle quadrotor transit operations under potentially risky wind gust conditions. Since the early foundational research from Schouwenaars *et al.* [2] and Richards and How [3], the collection of studies exploring centralized as well as decentralized Mathematical Programming (MP) or Mathematical Optimization-driven solutions for multi-vehicle motion planning problems (MVMPs) in ground [4], underwater [6, 7], and aerial robot applications [8, 9] has expanded steadily. Mixed-integer nonlinear programs (MINLPs) prove effective at encompassing the full set of MVMP constraints [28]. However, resolving such MINLPs for MVMP scenarios demands substantial computational resources (NP-hard), thereby hindering practical real-time use and large-scale deployment [10]. A practical method to address this limitation relies on receding-horizon (RH), or model predictive control (MPC) approaches [29, 30]. These approaches have demonstrated strong suitability for online, real-time trajectory generation in multi-robot teams navigating dynamic, partially known environments [11, 12]. Among the important strengths of MP-driven strategies is their support for detailed examination of the balance between mobility aspects (speed, acceleration, waypoints) and wireless communication parameters (bandwidth, buffer size, path loss, delay), as well as overall energy usage [8, 13]. In this study, the distributed MINLP-based motion planner is evaluated across several quadrotors, in which each vehicle calculates its own future path locally and shares it with neighboring units.

The main contributions of this study are as follows:

• An RH-MINLP and CBF-based framework for real-time, MVMP of multiple, networked quadrotors, operating outdoors in the presence of wind gusts. The resulting optimization problem is solved using a fast MINLP solution approach that combines Simulated Annealing and Interior point methods.

• Real-time validation of the framework with Hardware-in-the-loop (HWIL) experiments, followed by outdoor field tests featuring up to 6 DJI M100 quadrotors.

• Integration of the Dryden wind gust model with RH-MINLP and CBFs to perform realistic simulations (featuring up to 50 quadrotors) and HWIL testing with DJI Matrice M100 quadrotors. Source code is available at https://github.com/radlab-sketch/ (accessed on 24 December 2022).

Extensive performance results of the proposed framework are documented in this study.

Preliminaries

Quadrotor motion and paths

This section examines a set of n interconnected quadrotors functioning across well-specified inertial (East-North-Up (ENU)), body, and body-fixed reference frames. Every quadrotor i=1,…,n possesses an initial (origin) position oi together with a final (goal) position ei. O stands for the complete collection of origin positions, where $oi \in O$ for i=1,…,n. Similarly, E represents the full collection of goal positions, where $ei \in E$ for i=1,…,n. The straight-line separation between any quadrotors i and j appears as dij, for i=1,…,n with $j \neq i$.

All quadrotors need to preserve a minimum clearance of $d$safe to ensure mutual collision avoidance. In the case of each quadrotor i, Gaussian quadrature serves to compute the complete arc length of its trajectory, labeled as Ui. Along this defined trajectory, the linear velocity si and rotational velocity ωi of quadrotor i are defined in the vehicle's body-fixed frame. At any moment t, the position p(t) = (xi(t), yi(t), zi(t)) indicates quadrotor i's coordinates in the NED frame while

© 2025 The Author(s). | Published by Agro Intelligence Research Press

following its trajectory, obtained directly from the velocity profile $si(t)$. For each quadrotor i, its trajectory appears as a three-dimensional piecewise 7th order spline curve $\mathbb{SP}(u)$, in which u corresponds to the normalized arc length parameter along this curve. Construction of these curves involves the fusion of three one-dimensional, piecewise 7th-order splines. Such piecewise 7th order spline curves maintain continuity across the first derivatives (slope), second derivatives (curvature), third derivatives (jerk), and fourth derivatives (snap) for the entire length of the trajectory. **Figure 2** shows the spline curve trajectories corresponding to a 6-quadrotor setup.

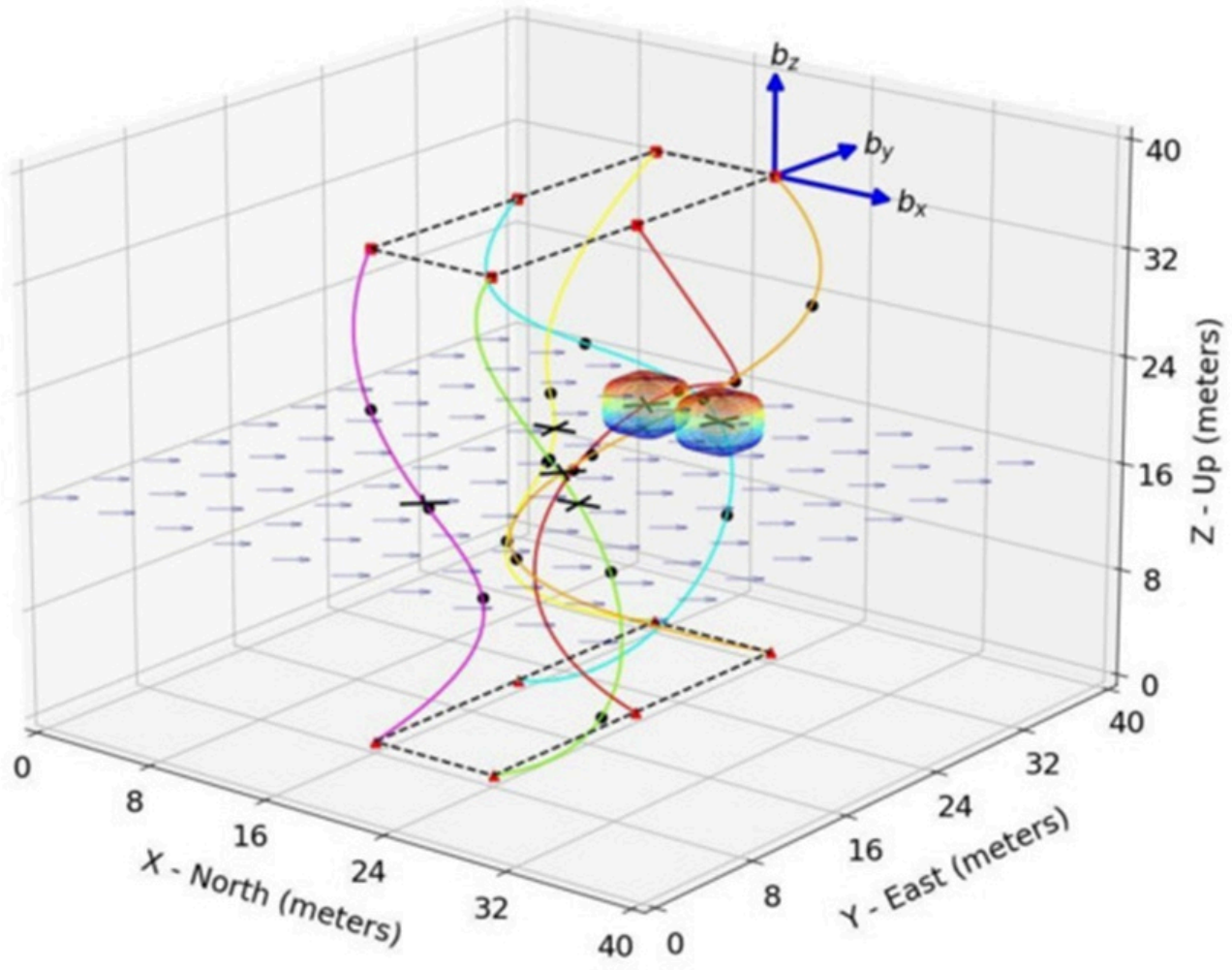

Figure 2. Depiction of a multi-quadrotor scenario involving six vehicles progressing along their spline trajectories (illustrated via solid, colored lines) while encountering wind effects. Control Barrier Functions (CBFs), along with their corresponding safety certificates rendered as super-ellipsoids, facilitated collision prevention against wind-induced disruptions during movement. The vector field (blue arrows) depicts spatially inhomogeneous wind gusts generated by the Dryden wind model at a height of 15 m. Red triangular and square markers designate the initial and terminal points of the spline paths, arranged in a patterned layout. Black round markers highlight the spline-path waypoints. The inertial reference frame together with the body frame (bx, by, and bz) is displayed. The quadrotors appear here functioning inside a 40 m × 40 m × 40 m airspace.

The differential flatness inherent in quadrotor dynamics, the incorporation of 3-dimensional piecewise 7th-order spline curves, and the restrictions imposed on speed, acceleration, snap, and yaw rate yield a kinodynamically feasible velocity profile for quadrotors [31, 32]. An in-depth review covering spline curve formulation and assessment appears in Ref. [33]. Let (u) denote the curvature along the spline curve i. The angular speed (u) can be derived from the linear speed and spline curvature according to the subsequent expression:

© 2025 The Author(s). | Published by Agro Intelligence Research Press

$$\omega^{I}(u) = s^{I}(u)\,\kappa^{I}(u)\,. \quad (1)$$

Receding Horizon (RH)

Thor represents the timeframe of the receding horizon, selected based on the performance limits of the onboard flight planning and control hardware. At each discrete time moment t, every quadrotor determines its upcoming trajectory covering t+1 to t+Thor and transmits this trajectory to the other vehicles in the group. This trajectory appears as (t)= ($\mathbf{p}i$(t+1),…,$\mathbf{p}i$(t+Thor)). Only the immediate portion for time t+1 gets carried out, with the entire planning cycle beginning anew at the next time step t+1. Mission completion occurs at time step Tmission once the final quadrotor arrives at its destination. Any quadrotor arriving ahead of Tmission stays in a fixed hover position at the goal until the entire operation finishes.

Communication modeling and ordering

All quadrotors feature a mobile ad hoc network (MANET) transmitter for distributing RH-MINLP results within the group. MANET links function via immediate single-hop ties or multi-hop forwarding, creating a fully interconnected network. Sequential wireless exchanges use a round-robin scheduling method to promote balanced bandwidth sharing in MANETs and improve system resilience. The quadrotor order within the round-robin cycle gets assigned randomly before mission launch. The initial quadrotor listed in this cycle also executes the first departure.

Dryden wind model and spline regeneration

A continuous Dryden turbulence representation simulates gusts and assesses their impact on motion planning outputs [34]. The pioneering open-source version of this Dryden wind turbulence representation was introduced in Ref. [35]. As gusts push quadrotors away from their preset spline trajectories, an efficient spline regeneration routine provides each vehicle with a revised spline trajectory that originates from the current offset position and points toward the target. This spline regeneration appears demonstrated in the attached video file.

Control barrier functions and safety barrier certificates

A super-ellipsoidal Exponential Control Barrier Function (ECBF) encloses every quadrotor, as shown in **Figure 2**. For any duo of quadrotors (i,), the pairwise protected zone $\mathcal{B}ij$ and the pairwise super ellipsoid h(qi,qj) receive formulation as:

$$\mathcal{B}^{ij} = \left\{ \left(q^{i}, q^{j}\right) \middle| h^{ij}\left(q^{i}, q^{j}\right) \geq 0 \right\}, \quad (2)$$

$$h^{ij}\left(q^{i}, q^{j}\right) = \left(x^{i} - x^{j}\right)^{4} + \left(y^{i} - y^{j}\right)^{4} + \left(\frac{z^{i} - z^{j}}{c}\right)^{4} - d_{safe}^{4} \quad (3)$$

Where qi represents the full state of the quadrotor i, $d$safe is the safety distance, and c is the scaling factor along the Z-axis caused by airflow disturbance from the downwash of one quadrotor flying over another quadrotor. In this study, the quadrotors flew at a safe distance from each other along the vertical direction. As such, c was chosen to be equal to one (1). The two quadrotors are considered safe when the two super-ellipsoids do not intersect. Readers are referred to Ref. [36] and its references for information about the mathematical construction, verification, and incorporation of ECBFs in motion planners through the use of Quadratic Programming (QP).

Optimization Model

© 2025 The Author(s). | Published by Agro Intelligence Research Press

Each quadrotor addresses the optimization (MINLP) issue (t) detailed in (4)–(14). Optimization targets the speed si along the assigned trajectory, employing supporting variables for position (xi, yi, zi), arc length (ui), acceleration (ai), and communication links (Cij, $j \neq i$). While resolving (t), the quadrotor i incorporates the latest available trajectories from every other vehicle.

Problem Size:

(t) involves (n+5)hor decision variables, (2n+5)Thor constraints, and variable bounds. Problem dimensions increase proportionally with quadrotor count n.

Objective function

Objective function (4) drives the quadrotors to minimize the cumulative distance (arc length) separating their current positions from the target over the entire receding horizon. This prioritizes the progress of the vehicles toward their assigned destinations.

$$\begin{aligned} \underset{s,x,y,z,u,a,C}{\text{minimize}} \quad & \sum_{k=t+1}^{t+T_{hor}} \left(U^t - u^t(k)\right) \\ \text{subject to} \quad & \forall k \in \{t+1, \ldots, T_{\text{hor}}\} \end{aligned} \tag{4}$$

$$\left(x^t(k), y^t(k), z^t(k)\right) = \mathbb{SP}^t\left(u^t(k)\right) \tag{5}$$

$$u^t(k) = u^t(k-1) + s^t(k)\,\Delta t \tag{6}$$

$$u^t(t) \leq u^t(k) \leq U^t \tag{7}$$

$$s^t(k) = s^t(k-1) + a^t(k)\,\Delta t \tag{8}$$

$$s_{\min} \leq s^t(k) \leq s_{\max} \tag{9}$$

$$\begin{aligned} & a_{\min} \leq a^t(k) \leq a_{\max} \\ & \forall j \in \{1, \ldots, n\}, j \neq i \end{aligned} \tag{10}$$

$$\left(d^{ij}(k)\right)^2 \geq d_{\text{safe}}^2 \tag{11}$$

© 2025 The Author(s). | Published by Agro Intelligence Research Press

Path (Kinematic) constraints

Constraints (5)–(7) establish the vehicle's placement on its trajectory. Placement receives description via two approaches: distance covered along the trajectory (ui) and spatial coordinates (xi,,). The first method supports kinematic and dynamic rules, whereas the second calculates straight-line separations for avoidance and linkage. Constraint (5) establishes the 7th-order spline curves $\mathbb{SP}(ui(k))$ uniting these variable categories. Starting from its placement at planning initiation, constraint (6) adjusts the arc length per time step in line with the vehicle's speed. Δt corresponds to the DJI Matrice M100 flight controller refresh interval recorded in field trials. Constraint (7) confirms the quadrotor remains confined between its starting planning spot and final goal throughout.

Speed and acceleration (Dynamic) constraint

From the quadrotor's initial linear speed si at planning onset, constraint (8) progresses this speed stepwise using acceleration ai. Constraints (9)–(10) act as dynamic limits, ensuring that linear speed (and resulting angular speed) and acceleration remain within proper ranges per time step for each vehicle. These ranges are based on the DJI M100 capabilities and spline curvature to avoid motor overload. Because 7th-order spline curves arise from snap (4th-derivative) minimization, trajectories enable fluid tracking. Angular speed matching the best linear speed stays attainable via the linkage in (1).

Collision avoidance constraint

Non-convex constraint (11) sets the essential minimum separation $d$safe among all quadrotor pairs continuously to block impacts.

$$C^{ij}(t) = \begin{cases} 1, & \text{if } d^{ij} \leq \eta_d, \\ 0, & \text{otherwise.} \end{cases} \quad (12)$$

Communication connectivity constraint

Binary variable (t) denotes if a pair of quadrotors falls inside one-hop range ηd, according to this equation:

Optimization Solution Technique

The computational strategy for addressing (4)–(14) breaks down into three distinct layers: the topmost layer, the central layer, and the bottom layer.

Given the involvement of several independent agents (namely, numerous quadrotors), the topmost layer defines the foundational setup for collective distributed choices, covering decision sequence and corresponding trajectory details at each time step t.

The central and bottom layers draw on proven computational strategies for mixed-integer nonlinear programming (MINLP) [37, 38]. Within the central layer, the process manages the discrete components and linkage stipulations in each quadrotor's issue (t) by employing Simulated Annealing (SA). This SA mechanism locks in the discrete component, transforming the leftover portion into a continuous nonlinear program. Resolution of this fundamental continuous nonlinear program then takes place in the bottom layer using interior-point techniques, which determine the velocity for each quadrotor over the time interval.

Outer level: Distributed decision making

© 2025 The Author(s). | Published by Agro Intelligence Research Press

Mutual communication access exists among all quadrotors at time 0. As described previously, a round-robin system dictates the sequence of choices and information sharing among the vehicles. Assignment of this sequence may occur randomly or through advanced determination. For simplicity and without restricting generality, the sequence takes the form 1,…,n.

At time t, quadrotor i tackles the issue (t+1) in succession, factoring in these trajectories:

· Trajectories $\mathcal{P}j(t+1)$ belonging to quadrotors $j<i$, given that those vehicles have already produced their fresh trajectories, and

· Trajectories (t) belonging to quadrotors $j>i$, given that those vehicles have not yet produced their fresh trajectories.

When (t+1) yields a workable result, the fresh trajectory takes shape as (t+1). When no workable result emerges, the vehicles hover in place for protection pending human intervention. Subsequently, every trajectory undergoes transmission to the other vehicles.

Middle level: Simulated annealing for discrete variables and communication constraints

Resolution of (t+1) for individual quadrotor i at every time step t becomes necessary under the topmost layer. Linkage components, together with linkage stipulations (12), substantially increase the processing requirements of (t+1): these components arexist in binary format, totaling $n*T$hor per instance (with other components remaining independent of group size), alongside $n*T$hor linkage stipulations per instance. With group size n increasing, the Big-M linkage stipulations, which incorporate integers and the parameter M, pose significant computational challenges during the search for workable outcomes [39]. The central layer within the computational procedure confronts this processing challenge to enable real-time outcomes.

Selection of a fitting procedure for linkage components and stipulations begins with recognizing that any workable outcome for (t+1) supports direct execution irrespective of its optimality level. Procedurally speaking, a recognized technique such as branch-and-bound (BB), which involves extensive exploration, can tackle MINLPs [40, 41]. However, this may still require several RH-MINLP resolutions (and hence additional processing time) before securing a workable outcome, especially as dimensions increase.

Conversely, Simulated Annealing (SA) [42] is a probabilistic technique that can swiftly locate practical, workable solutions within MINLPs [43, 44]. Critical aspects for SA include the neighbor selection mechanism around the current best solution and the appraisal of the effectiveness of the outcome. During each SA cycle, sampling covers a modest quantity of neighbors surrounding the current solution (referred to as the “incumbent”). Replacement of the incumbent by any neighbor occurs with probability 1 upon superiority or with probability $exp-\Delta/Temp$ upon inferiority, wherein Δ captures the shift in outcome effectiveness, and $Temp$ stands for the prevailing system temperature. Reduction of $Temp$ happens across every SA cycle, fostering convergence toward a robust incumbent in the concluding stages. Termination of the procedure arises once $Temp$ reaches a sufficiently low value or a duration cap activates.

Sampling neighbors approach

Per the outline in **Algorithm 1**, selections of binary values for linkage components aimed at securing or boosting outcome workability. Condition Cij=0 fails to consistently signal that quadrotors i and j sit outside linkage reach. Instead, this condition indicates that proximity between the vehicles is unnecessary. Incumbent outcomes fulfilling the $n$conn stipulation precisely demonstrate that vehicles must uphold at least $n$conn connections, as opposed to an exact count. Illustration of this technique for producing a neighbor to the incumbent outcome over N waypoints appears in **Algorithm 1**.

© 2025 The Author(s). | Published by Agro Intelligence Research Press

1: **Input**: The sets $\{1,\ldots,-1\}$ and $\{1,\ldots,Thor\}$, $\mathcal{C}k'$

2: **Output**: $\mathcal{C}k'$

3: Randomly select $k' \in \{1,\ldots,Thor\}$.

4: Randomly select $j' \in \mathcal{C}k'$ and $j'' \notin \mathcal{C}k'$.

5: Set $C^{ij'}(k')=0$, $C^{ij''}(k')=1$.

6: Update: $\mathcal{C}k' \leftarrow \mathcal{C}k' \setminus j' \cup j''$.

Algorithm 1. Generating a neighbor of an incumbent solution for Simulated Annealing

4.2.2. Evaluating solution quality

Following fixation of linkage components and fulfillment of stipulation (13), a compacted variant of (t), termed $\mathcal{O}i$reduced(t), arises by substituting rules (12)–(14) with

$$\left(d^{ij}(k)\right)^2 \leq \eta_d^2 \ \text{ if } \ C_{ij}(k) = 1 \quad (13)$$

SA adopts the objective function value of $\mathcal{O}i$reduced(t) as its effectiveness gauge (assigning ∞ to any unsolvable case).

Additionally, $\mathcal{O}^i_{reduced}(t)$ encounters diminished processing loads amid n growth in comparison with (4)–(14) because of eliminated big-M stipulations and integer components.

Reduced problem size

This emerging optimization issue proves markedly more compact, containing 5$\mathcal{T}$hor variables along with (N+$nconn$+4)hor constraints.

Lower level: Nonlinear optimization

$\mathcal{O}i$reduced(t) forms a nonlinear, non-convex program resolvable via an interior-point approach for nonlinear optimization adapted from [45]. Consultation of Ref. [45] and associated materials offers deeper insight into this nonlinear optimization procedure.

Results and Discussion

© 2025 The Author(s). | Published by Agro Intelligence Research Press

Implementation of the RH-MINLP structure spanned numerical simulations, HWIL, plus outdoor flight trials. Realization in Python 3.7 covered the optimization model $\mathcal{O}i$, the full three-layer optimization procedure, and CBFs. Python-based specialized routines produced minimum-snap 7th-order splines traversing N predetermined waypoints. The Dryden representation for wind gust creation was implemented on the ground station computer using Python.

A desktop machine powered by numerical simulations, featuring a Lenovo i5-6400 Intel CPU running at 2.70 GHz with a quad-core architecture and 8 GB RAM. Deployment in HWIL and outdoor flight trials involved DJI M100 quadrotors equipped with Raspberry Pi 4 computers (Quad-core Cortex-A72 ARM v8 64-bit SoC operating at 1.5 GHz with 4 GB RAM). Inclusion on every quadrotor came in the form of a transceiver radio unit operating in the 915 MHz unlicensed band, supporting half-duplex bidirectional RF connections at up to 300 Kbps. Participation in the MANET extended to a ground station machine (Lenovo Intel Dual Core i5 processor at 3.3 GHz with 8 GB RAM), which maintained a web-oriented interface handling operation setup, temporal alignment, and operation transfer. Positional precision and sampling frequency for the GPS sensor aboard the DJI M100 equal 1 m (on average) and 4 Hz. Acquisition of state feedback (current positions and velocities) relied on sampling the integrated telemetry stream from the DJI M100 at 50 Hz. Powering the quadrotors was the TB48D battery possessing 5700 mAh capacity [46]. **Table 1** summarizes essential motion and linkage parameters employed across HWIL, numerical simulations, and field trials.

Table 1. Motion and communication parameters used in HWIL, numerical simulations, and field tests.

$d$safe	3 m	$s$min	0	$s$max	0.5 m/s
$amin$	−0.25 m/s2	$a$max	0.25 m/s2	$nconn$	1
ηd	5 m	Ptr	100 mW	Thor	3

Execution of HWIL trials utilized the DJI Assistant 2 flight emulation software. Real-time replication of telemetry outputs and velocity yaw rate commands fed into the DJI N1 flight controller matched rigid body dynamics with the DJI M100. Placement during HWIL trials positioned the vehicles and ground station in a linear arrangement, with nearly 0.5 m gaps between individual vehicles and nearly 1.5 m between the ground station and the vehicles.

Connection of the Python code to live DJI M100 telemetry was via UART, using a Linux SDK from the DJI M100 N1 flight unit. Velocity computed via resolution of $\mathcal{O}$ functioned as the reference target for the DJI M100 N1 flight controller, prompting appropriate control actions to attain that target. Outdoor trials incorporated a manual pause feature to immobilize the vehicle until human command takeover in situations of weakened MANET effectiveness (average vehicle-to-vehicle wireless delay exceeding 0.33 s), intense wind gusts (exceeding 18 m/s), or dangerously depleted battery levels (below 5% power).

Focus on numerical simulations that probe expandability (up to 50 quadrotors) of the RH-MINLP + CBF structure, while contrasting processing performance between the SA + Interior Point Method procedure and another standard technique (Branch-and-Bound (BB) + Interior Point Method). HWIL trials engaged up to 6 DJI M100 units to examine (1) wind disruption impacts upon safety breaches, (2) protection levels delivered by CBFs, and (3) combined wind disruption and CBF influences upon Tmission. Validation of live feasibility for the RH-MINLP + CBF method in gusty outdoor conditions followed through actual flight trials after completing simulations and HWIL trials.

All flights within numerical simulations, HWIL trials, and outdoor trials took place inside a 40 m × 40 m × 20 m airspace, encompassing these three subtasks:

· Take-off and Formation: Vehicles departed in sequence and advanced to a designated area for arrangement into a patterned layout. Sample initial layouts included a straight line, a triangle, and a rectangle, as depicted in **Figure 1**. The layout's starting altitude was 12.5 m above ground level (AGL).

© 2025 The Author(s). | Published by Agro Intelligence Research Press

· Waypoint-based Transit: Following layout formation, vehicles initiated movement to retain the flight layout while traversing 5 waypoints distributed throughout a 40 m × 40 m × 20 m zone.

· Return-To-Home (RTH): Completion of all waypoint visits triggered sequential RTH maneuvers for safe descent back to departure locations.

The definition of principal assessment measures follows:

· Tmission: denotes the transit time between the start of the multiple quadrotor formation and their return to their start points, averaged over multiple runs.

· nCBF: number of CBF activations averaged over multiple runs and rounded to the nearest integer.

· Tcomp: Solver computation time averaged over all quadrotors, further averaged over multiple runs.

· RR: Optimization-based motion-plan re-planning rate in Hz, average over multiple runs.

· Tsaving: denotes the percentage of Tcomp time saved when using SA instead of the BB method.

· Dobj−gap: denotes the percentage gap in the objective function values (as defined by (4)) between BB and SA.

Repetition of each numerical simulation occurred five (5) times, HWIL experiments nine (9) times, and outdoor flight tests five (5) times. Application of Dryden gusts with an average speed of 9 m/s and a standard deviation of 1.23 m/s was performed in numerical simulations and HWIL.

HWIL: Flight safety accorded by CBFs

With $d$safe held constant, **Figure 3** (top) presents the frequency at which inter-vehicle separation (dij) fell short of $d$safe under gusty environments. Such genuine safety breaches emerged because gusts deflected the vehicles from their designated routes, notwithstanding repeated $\mathcal{O}$ computations. This pattern emphasizes the necessity for supplementary protective layers to avert mid-air impacts.

© 2025 The Author(s). | Published by Agro Intelligence Research Press

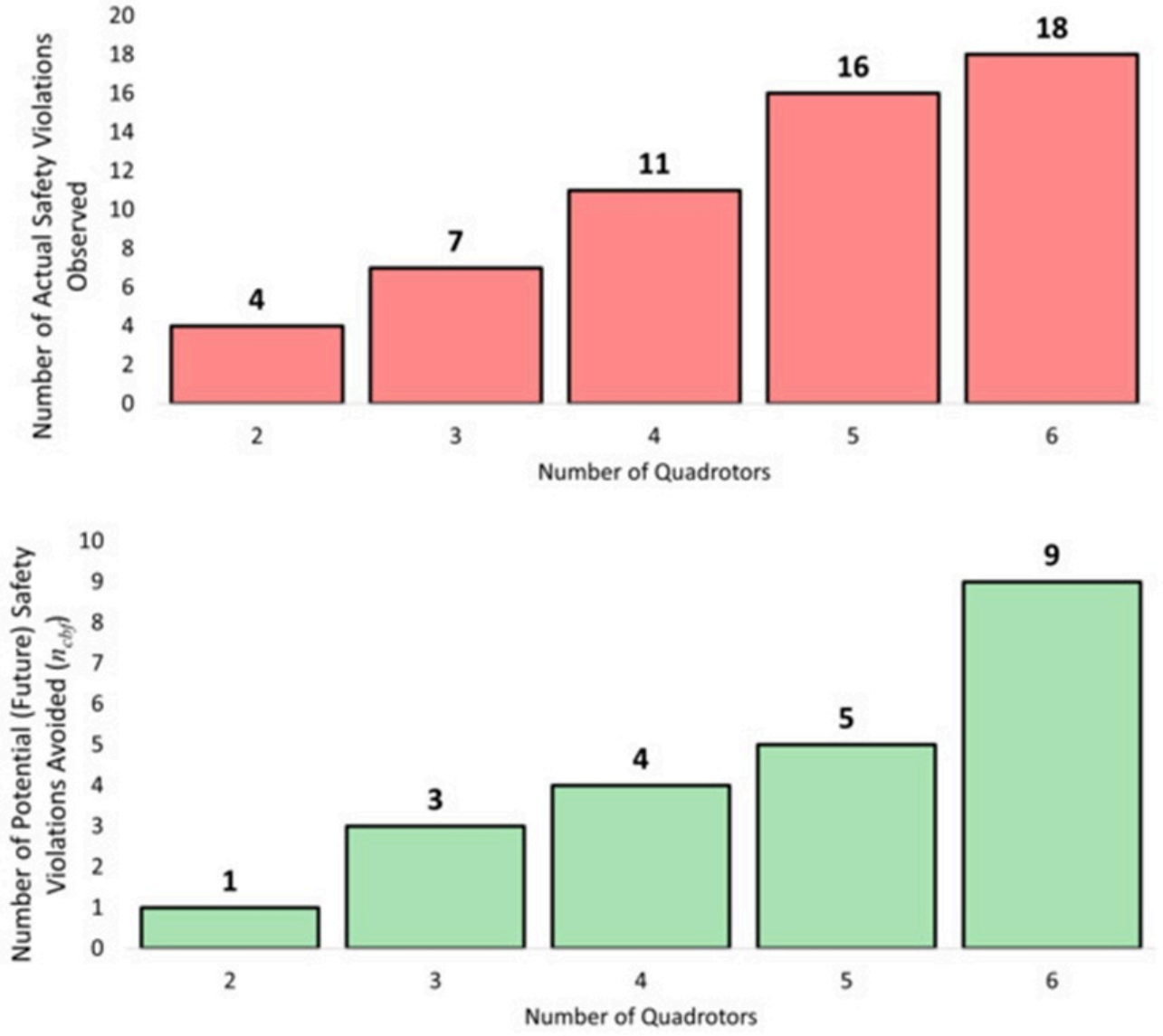

Figure 3. (Top) In HWIL tests without CBF, the number of actual safety violations is shown in the red bars. As CBFs were not used, none of these actual safety violations could be avoided. (Bottom) In HWIL tests with CBF, the number of CBF-activations nCBF is shown in the green bars. Each of these CBF activations helped the quadrotors to avoid potential future safety violations. As a result, the use of CBFs did not lead to any actual safety violations. Data averaged over nine runs.

Following the integration of CBFs into the trajectory generation workflow, as illustrated in **Figure 3** (bottom), genuine safety breaches were zero (0) throughout flights in gusty conditions. This indicates that numerous prospective safety risks were preempted via CBF interventions.

Furthermore, the volume of prospective safety risks mitigated by CBF inclusion was considerably smaller than in configurations lacking CBFs. The reason lies in the vehicles pursuing more secure paths starting immediately upon mission initiation due to CBF engagement. As a result, subsequent stages encountered a comparatively modest quantity of prospective safety risks. Importantly, in the complete absence of Dryden wind gusts, $\mathcal{O}$ solving produced no safety breaches whatsoever.

© 2025 The Author(s). | Published by Agro Intelligence Research Press

HWIL: Effect of wind disturbances and CBFs on $\mathcal{T}mission$

Holding $d$safe constant, **Figure 4** displays shifts in $\mathcal{T}$mission both with and without wind disruptions. Observations confirm that $\mathcal{T}$mission grows markedly when Dryden wind gusts are active, as $\mathcal{O}$ requires more repeated resolutions (since gusts displace vehicles from planned routes).

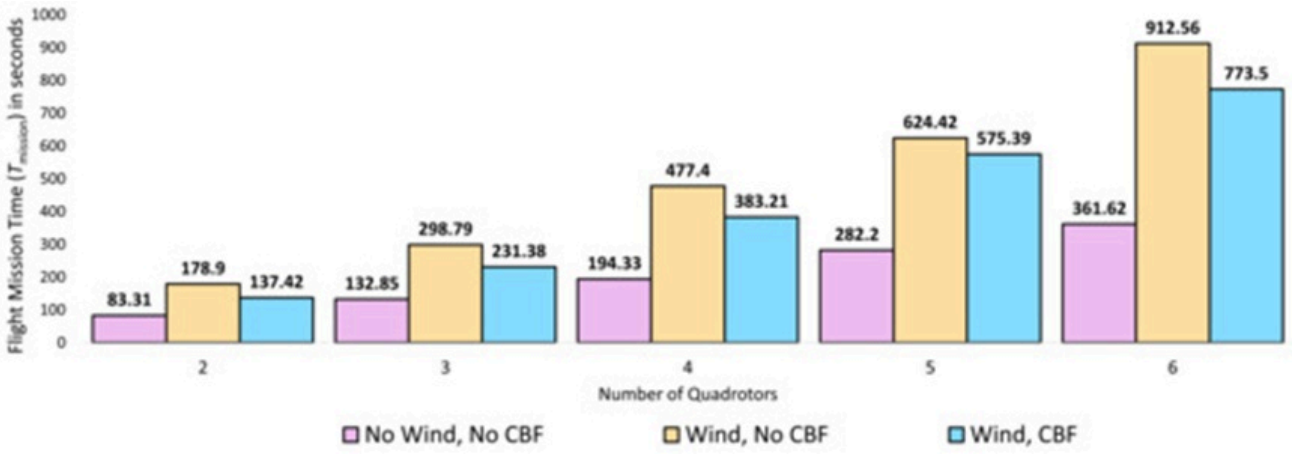

Figure 4. For $d$safe = 3 m, the above charts depict $\mathcal{T}$mission in seconds for different HWIL scenarios. The presence of wind increases the computational times and results in severe safety violations. Adding CBFs to the overall motion planning strategy reduces computational time while resulting in zero safety violations. Data averaged over nine runs.

Figure 4 additionally charts modifications in $\mathcal{T}$mission during wind disruptions when CBFs are active (blue-colored data series). Results show $\mathcal{T}$mission rises under CBF usage in gusty settings versus calm conditions. Nevertheless, CBF presence yields a reduced $\mathcal{T}$mission relative to scenarios without any CBFs. This stems from CBF actions delivering collision protection right at mission commencement, which decreases the overall instances of $\mathcal{O}$ resolution. The shortened $\mathcal{T}$mission correspondingly lowered battery expenditure by the vehicles. Averaged over the 9 runs, the battery savings per quadrotor for the 2, 3, 4, 5, and 6 quadrotor tests were 25.14%, 20.39%, 18.52%, 11.81%, and 16.4%, respectively.

Numerical simulations for scalability

Simulations extended up to 50 quadrotors in simulated outdoor conditions to evaluate processing expandability amid Dryden wind gusts. **Table 2** summarizes findings across these configurations. The SA + interior-point computational strategy was benchmarked against a BB + interior-point strategy as outlined in Refs. [40] and [41].

Table 2. Numerical simulation results to study the scalability of the RH-MINLP framework. Data averaged over 5 runs.

N	BB			SA		
	$\mathcal{D}$obj-gap	$\mathcal{T}$saving	nCBF	$\mathcal{T}$comp	nCBF	$\mathcal{T}$comp
10	−5.29%	47.54%	16	195.2	14	132.3
15	−4.66%	66.97%	19	311.9	17	186.8
20	0.2%	139.21%	18	648.5	19	271.1
25	−3.10%	135.06%	21	902.4	22	383.9
30	−1.98%	144.83%	30	1376.2	27	562.1
40	−7.81%	182.52%.	31	2314.7	31	819.3

© 2025 The Author(s). | Published by Agro Intelligence Research Press

50	−6.52%	231%	42	3920.7	38	1184.5

Across all configurations, both nCBF and Tcomp rise in tandem with n. This escalation becomes especially evident at elevated n values because of greater collision likelihoods together with growth in the quantity of variables and constraints inside $\mathcal{O}$.

SA demonstrates clear superiority over BB concerning Tcomp, as reflected in Tsaving figures. Such Tcomp reductions arise since BB only secures portions of the binary variables (retaining others as continuous values spanning 0 to 1) in each iteration. Consequently, the nonlinear solver encounters more extensive issues under BB than under SA. Still, upon termination, BB achieves stronger objective function outcomes in every test aside from n = 20. This aligns with expectations given BB's concentration on global optimality. As quadrotor quantities grow, BB risks failing to complete within real-time constraints, whether due to the sheer scale of the problem or the non-convexity of the fundamental nonlinear issue driven by collision-prevention rules. By contrast, SA serves as an exploratory heuristic that prioritizes securing workability initially before enhancing the objective function value, allowing termination to satisfy real-time constraints.

Outdoor flight tests

Real-world outdoor trials engaged up to 6 DJI M100 quadrotors to verify the RH-MINLP + CBF structure. Testing took place in an expansive park setting in Philadelphia. Gust intensities throughout the trials were recorded using an FT205 ultrasonic anemometer mounted to one DJI M100 quadrotor via a 20-inch 3D-printed extension, as shown in **Figure 1**. The FT205 operated at a 2 Hz sampling rate. Wind data gathering occurred while the instrumented vehicle hovered at 12.5 m above ground level. This vehicle maintained roughly 50 m separation from the main group to ensure protection. In the trial involving 2 quadrotors, the average wind speed was 12.23 m/s, with a standard deviation of 3.49 m/s. For the trial with 3 quadrotors, average wind speed stood at 10.33 m/s with a 1.54 m/s standard deviation. In the trial with 6 quadrotors, the average wind speed was 13.5 m/s, with a standard deviation of 2.0 m/s.

Figure 1 depicts snapshots of 2-, 3-, and 6-quadrotor tests. **Table 3** depicts the average Tmission, nCBF, Tcomp, and re-planning rate (RR). Tcomp varied from 26.8 ms to 74.6 ms. Re-planning rates ranged from 12 Hz to 30 Hz.

Table 3. Outdoor flight test results demonstrate the feasibility of the RH-MINLP + CBF framework. Data averaged over 5 flight tests per n.

n	Wind Speed (mean, stdev) (m/s)	RR (Hz)	Tcomp (ms)	nCBF	Tmission (s)
2	12.23, 3.49	30	26.8	1	141.52
3	10.33, 1.54	24	37.2	2	258.10
6	13.5, 2.0	12	74.6	4	829.47

The attached video provides visual documentation of these trials. During the 2-quadrotor trial, CBF engagement occurred as the vehicles completed a concentric-spiral route task and approached the separation threshold. One vehicle transitioned to hover, enabling the other to proceed safely. Analogously, the 3-quadrotor trial triggered CBF activation on two occasions, each involving a unique pair. For the 6-quadrotor trial, activation of 4 CBFs took place across assorted pairs whenever gusts brought vehicles into proximity.

Discussion

Owing to the fundamentally distributed nature of decision-making, decisions made by certain quadrotors can occasionally complicate or render unsolvable the coordination task for fellow vehicles. On select occasions, altering the decision

© 2025 The Author(s). | Published by Agro Intelligence Research Press

sequence produced better collective outcomes. Protection is assured at all times, as vehicles retain the option to hover in place when encountering unsolvable situations.

Despite deploying CBFs as an additional protective layer for collision prevention, ensuring complete collision resilience is complex, given the nonlinear behavior in the multi-UAV setup and unpredictable gusts. Subsequent efforts will examine robust control barrier functions aimed at bounded stabilization of the multi-UAV setup, as referenced in Ref. [27].

Although infrequent, meeting communication stipulations may occasionally cause network divisions. Methods for addressing these uncommon events are presented in Ref. [47].

As visible in **Figure 4**, growth in quadrotor numbers narrows the gap between Tmission absent CBFs and Tmission with CBFs. The effectiveness of CBFs in large-scale multi-robot operations remains an unresolved topic for further exploration [48].

Conclusion

This study confirmed the effectiveness of a distributed RH-MINLP + CBF motion planner designed for groups of quadrotors navigating gusty outdoor settings. Confirmation derived from numerical simulations, HWIL setups, and actual outdoor flight trials. Development of an innovative three-layer optimization solver incorporating Simulated Annealing accelerated the resolution procedure, yielding practical real-time trajectory generation. Integration of the Dryden wind gust representation injected authentic wind influences into the simulations and HWIL activities. CBF deployment provided defense against safety breaches and potential in-flight impacts from wind effects, thereby shortening overall mission durations. Outcomes from both simulations and physical trials highlighted notable reductions in processing time achieved by the SA-driven solver relative to a conventional benchmark technique, thereby illustrating the scalability of the proposed structure. Upcoming research will target integrating live wind gust assessments into the planning stage through non-sequential MANET exchange methods, along with refinements to the neighbor generation process in Algorithm 1 that draw upon real-time separations and historical trajectories.

Acknowledgements

None

Conflict of interest

None

Financial support

Funding for this work came from Lockheed Martin Advanced Technology Laboratories, Drexel University, and the New Jersey Institute of Technology through multiple internal research and development (IRAD) grants.

Ethics statement

None

Received: 29 Jan 2024 Revised: 04 Apr 2024 Accepted: 19 Apr 2024
Published online: 25 November 2025

© 2025 The Author(s). | Published by Agro Intelligence Research Press

Rights and permissions

Open Access The author(s) retain copyright. This article is licensed under the Creative Commons Attribution-NonCommercial-ShareAlike 4.0 International License. It may be shared and adapted for non-commercial purposes with appropriate attribution, an indication of changes, and distribution of adaptations under the same license. Third-party material may be subject to separate terms identified in its credit line. View the license at https://creativecommons.org/licenses/by-nc-sa/4.0/.

References

1. Causa F, Franzone A, Fasano G. Strategic and tactical path planning for urban air mobility: Overview and application to real-world use cases. Drones. 2023;7:11.

2. Schouwenaars T, De Moor B, Feron E, How J. Mixed integer programming for multi-vehicle path planning. In: Proceedings of the 2001 European Control Conference (ECC); Porto, Portugal; 2001. p. 2603-8.

3. Richards A, How JP. Aircraft trajectory planning with collision avoidance using mixed integer linear programming. In Proceedings of the 2002 American Control Conference (IEEE Cat. No.CH37301), Anchorage, AK, USA; 2002;3:1936–41.

4. Rezende AM, Goncalves VM, Pimenta LC. Safe coordination of robots in cyclic paths. ISA Trans. 2021;109:126-40.

5. Luo Y, Lu J, Zhang Y, Zheng K, Qin Q, He L, et al. Near-ground delivery drones path planning design based on BOA-TSAR algorithm. Drones. 2022;6:393.

6. Abichandani P, Torabi S, Basu S, Benson HY. Mixed integer nonlinear programming framework for fixed path coordination of multiple underwater vehicles under acoustic communication constraints. IEEE J Ocean Eng. 2015;40:864-73.

7. Wang T, Lima RM, Giraldi L, Knio OM. Trajectory planning for autonomous underwater vehicles in the presence of obstacles and a nonlinear flow field using mixed integer nonlinear programming. Comput Oper Res. 2019;101:55-75.

8. Shi W, Li J, Cheng N, Lyu F, Zhang S, Zhou H, et al. Multi-drone 3-D trajectory planning and scheduling in drone-assisted radio access networks. IEEE Trans Veh Technol. 2019;68:8145-58.

9. Zhao S, Wang X, Chen H, Wang Y. Cooperative path following control of fixed-wing unmanned aerial vehicles with collision avoidance. J Intell Robot Syst. 2020;100:1569-81.

10. Ragi S, Mittelmann HD. Mixed-integer nonlinear programming formulation of a UAV path optimization problem. In: Proceedings of the 2017 American Control Conference (ACC); Seattle, WA, USA; 2017. p. 406-11.

11. Abichandani P, Levin K, Bucci D. Decentralized formation coordination of multiple quadcopters under communication constraints. In: Proceedings of the 2019 International Conference on Robotics and Automation (ICRA); Montreal, QC, Canada; 2019. p. 3326-32.

12. Kuwata Y, Schouwenaars T, Richards A, How J. Robust constrained receding horizon control for trajectory planning. In: Proceedings of the AIAA Guidance, Navigation, and Control Conference and Exhibit; San Francisco, CA, USA; 2005. p. 6079.

13. Chiang WC, Li Y, Shang J, Urban TL. Impact of drone delivery on sustainability and cost: Realizing the UAV potential through vehicle routing optimization. Appl Energy. 2019;242:1164-75.

14. Cho DH, Ha JS, Lee S, Moon S, Choi HL. Informative path planning and mapping with multiple UAVs in wind fields. In: Distributed Autonomous Robotic Systems. Berlin/Heidelberg, Germany: Springer; 2018. p. 269-83.

15. Thibbotuwawa A, Bocewicz G, Radzki G, Nielsen P, Banaszak Z. UAV mission planning resistant to weather uncertainty. Sensors. 2020;20:515.

© 2025 The Author(s). | Published by Agro Intelligence Research Press

16. Patrikar J, Dugar V, Arcot V, Scherer S. Real-time motion planning of curvature continuous trajectories for urban UAV operations in wind. In: Proceedings of the 2020 International Conference on Unmanned Aircraft Systems (ICUAS); Athens, Greece; 2020. p. 854-61.

17. Jarray R, Bouallègue S, Rezk H, Al-Dhaifallah M. Parallel multiobjective multiverse optimizer for path planning of unmanned aerial vehicles in a dynamic environment with moving obstacles. Drones. 2022;6:385.

18. Military Standard. Flying Qualities of Piloted Aircraft; Technical Report MIL-STD-1797A; US Department of Defense: Fort Belvoir, VA, USA; 1990.

19. Moorhouse DJ, Woodcock RJ. Background Information and User Guide for MIL-F-8785C, Military Specification-Flying Qualities of Piloted Airplanes; Technical Report AFWAL-TR-81-3109; Air Force Wright Aeronautical Labs, Wright-Patterson Air Force Base: Dayton, OH, USA; 1982.

20. Rodriguez L, Cobano JA, Ollero A. Wind field estimation and identification having shear wind and discrete gusts features with a small UAS. In: Proceedings of the 2016 IEEE/RSJ International Conference on Intelligent Robots and Systems (IROS); Daejeon, Republic of Korea; 2016. p. 5638-44.

21. Abichandani P, Lobo D, Ford G, Bucci D, Kam M. Wind measurement and simulation techniques in multi-rotor small unmanned aerial vehicles. IEEE Access. 2020;8:54910-27.

22. Ames AD, Coogan S, Egerstedt M, Notomista G, Sreenath K, Tabuada P. Control barrier functions: Theory and applications. In: Proceedings of the 2019 18th European Control Conference (ECC); Naples, Italy; 2019. p. 3420-31.

23. Ghaffari A. Operational Safety Control for Unmanned Aerial Vehicles Using Modular Barrier Functions. In Proceedings of the 2020 American Control Conference (ACC), Denver, CO, USA; 2020. p. 1719–24.

24. Xu B, Sreenath K. Safe teleoperation of dynamic UAVs through control barrier functions. In Proceedings of the 2018 IEEE International Conference on Robotics and Automation (ICRA), Brisbane, Australia; 2018. p. 7848–55.

25. Lindemann L, Dimarogonas DV. Control barrier functions for multi-agent systems under conflicting local signal temporal logic tasks. IEEE Control Syst Lett. 2019;3:757-62.

26. Robey A, Hu H, Lindemann L, Zhang H, Dimarogonas DV, Tu S, et al. Learning control barrier functions from expert demonstrations. In: Proceedings of the 2020 59th IEEE Conference on Decision and Control (CDC); Jeju, Republic of Korea; 2020. p. 3717-24.

27. Jankovic M. Robust control barrier functions for constrained stabilization of nonlinear systems. Automatica 2018;96:359–67.

28. Israr A, Ali ZA, Alkhammash EH, Jussila JJ. Optimization methods applied to motion planning of unmanned aerial vehicles: A review. Drones. 2022;6:126.

29. Abichandani P, Mallory K, Hsieh MYA. Experimental multi-vehicle path coordination under communication connectivity constraints. In Experimental Robotics; Springer Tracts in Advanced Robotics Book Series; Springer: Berlin/Heidelberg, Germany; 2013. p. 183–97.

30. Abichandani P, Ford G, Benson HY, Kam M. Mathematical programming for multi-vehicle motion planning problems. In Proceedings of the 2012 IEEE International Conference on Robotics and Automation, Saint Paul, MN, USA; 2012. p. 3315–22.

31. Mellinger D, Kumar V. Minimum snap trajectory generation and control for quadrotors. In Proceedings of the 2011 IEEE International Conference on Robotics and Automation, Shanghai, China; 2011. p. 2520–5.

32. Richter C, Bry A, Roy N. Polynomial trajectory planning for aggressive quadrotor flight in dense indoor environments. In Robotics Research; Springer: Berlin/Heidelberg, Germany; 2016. p. 649–66.

© 2025 The Author(s). | Published by Agro Intelligence Research Press

33. Lepetic M, Klancar G, Skrjanc I, Matko D, Potocnik B. Time optimal path planning considering acceleration limits. Robot Auton Syst. 2003;45:199-210.

34. Hakim TMI, Arifianto O. Implementation of Dryden continuous turbulence model into Simulink for LSA-02 flight test simulation. J Phys Conf Ser. 2018;1005:012017.

35. Lobo D. Implementation of Dryden Wind Turbulence Model in Python. 2020. Source Code. https://github.com/radlab-sketch/drydenModelPython (accessed on 24 December 2022).

36. Wang L, Ames AD, Egerstedt M. Safe certificate-based maneuvers for teams of quadrotors using differential flatness. In Proceedings of the 2017 IEEE International Conference on Robotics and Automation (ICRA), Singapore; 2017. P. 3293–8.

37. Potra FA, Wright SJ. Interior-point methods. J Comput Appl Math. 2000;124:281-302.

38. Benson HY, Shanno DF. Interior-point methods for non-convex nonlinear programming: Regularization and warmstarts. Comput Optim Appl. 2008;40:143-89.

39. Bonami P, Lodi A, Tramontani A, Wiese S. On mathematical programming with indicator constraints. Math Program. 2015;151:191-223.

40. Lee J, Leyffer S. Mixed Integer Nonlinear Programming; Springer Science & Business Media: Berlin/Heidelberg, Germany; 2011;154.

41. Liberti L, Sager S, Wiegele A. Mixed-integer nonlinear optimization: A hatchery for modern mathematics. Oberwolfach Rep. 2020;16:1573-637.

42. Kirkpatrick S, Gelatt CD Jr, Vecchi MP. Optimization by simulated annealing. Science. 1983;220:671-80.

43. Cardoso M, Salcedo R, De Azevedo SF, Barbosa D. A simulated annealing approach to the solution of MINLP problems. Comput Chem Eng. 1997;21:1349-64.

44. Wei-zhong A, Xi-Gang Y. A simulated annealing-based approach to the optimal synthesis of heat-integrated distillation sequences. Comput Chem Eng. 2009;33:199-212.

45. Shanno D, Vanderbei R. Interior-point methods for non-convex nonlinear programming: Orderings and higher-order methods. Math Program. 2000;87:303-16.

46. Matrice 100 TB48D Battery. https://store.dji.com/product/matrice-100-tb48d-battery (accessed on 5 January 2023).

47. Abichandani P, Benson HY, Kam M. Multi-vehicle path coordination in support of communication. In: Proceedings of the 2009 IEEE International Conference on Robotics and Automation; Kobe, Japan; 2009. p. 3237-44.

48. Qin Z, Zhang K, Chen Y, Chen J, Fan C. Learning safe multi-agent control with decentralized neural barrier certificates. arXiv. 2021;arXiv:2101.05436.

© 2025 The Author(s). | Published by Agro Intelligence Research Press